Study on the corrosion resistance and durability of polymer coatings in high-temperature and high-humidity environments

Gabriel Jean[1], Agathe Léo[1,*]

[1]Department of Material Science, Universite de Strasbourg, France

***Corresponding Author:**
a.leo9872@gmail.com

Received: 11/10/2024
Revised: 12/01/2025
Accepted: 19/03/2025
Published: 30/04/2025

Abstract: Polymer materials are widely used in various industrial fields and serve as effective corrosion-resistant coatings. However, their performance in complex high-temperature, high-humidity corrosion environments remains to be evaluated. This study selected four mature corrosion-resistant coating systems from different manufacturers as test samples (MN-1 to MN-4) and prepared four test panels according to the coating requirements of each system. Concurrently, methods for pore analysis, corrosion resistance testing, and durability assessment of corrosion-resistant coatings were designed, forming the primary experimental research methods. The changes in the adhesion resistance to chlorine, sulfate ions, and carbon dioxide ions of the coatings on the surfaces of MN-1 to MN-4 under high-humidity conditions were compared to evaluate the overall corrosion resistance performance of the four coatings. Based on the corrosion resistance capabilities of the four coatings, a polymer sealant was prepared using a combination of raw materials. The six samples of the designed polymer sealant maintained an overall material weight within the range of 0.025–0.035 g under high-temperature and humid conditions, demonstrating strong resistance to aging.

Keywords: polymer coating, corrosion resistance, high-temperature and high-humidity environment, durability

1 | Introduction

Polymer coatings are protective layers formed on surfaces with a wide range of applications. They provide many important functions, such as corrosion resistance, wear resistance, waterproofing, and thermal insulation [1, 2, 3].

Polymer coatings play an important role in corrosion resistance [4]. During the production and use of various metal products, phenomena such as oxidation and corrosion caused by high temperatures and humidity can lead to a decline in material performance or even failure [5, 6, 7]. The function of polymer coatings is to form a protective layer that prevents metal materials from coming into contact with the external environment, thereby effectively extending their service life [8, 9]. For example, in automobile manufacturing, vehicle bodies coated with polymer coatings can effectively resist erosion from external environments such as acid rain and corrosive gases [10, 11]. Polymer coatings also play a critical role in wear resistance [12]. Many metal products undergo varying degrees of wear during use, such as mechanical parts and tools [13]. The hardness and

durability of polymer coatings make them an ideal material for protecting metal surfaces [14, 15]. For example, applying a polymer coating to industrial equipment can effectively reduce friction wear and extend the service life of mechanical parts [16]. Polymer coatings can also provide waterproofing functionality. In fields such as construction and shipbuilding, waterproofing issues often need to be addressed [17, 18]. Polymer coatings have excellent waterproofing properties, effectively preventing moisture from penetrating the metal surface and thus protecting the material from moisture corrosion [19, 20, 21]. For example, in construction, applying a polymer coating to exterior walls can effectively prevent rainwater penetration and keep the building dry [22]. Polymer coatings also have thermal insulation properties [23]. In applications requiring thermal insulation, polymer coatings can form an insulating layer that reduces heat conduction and radiation, thereby enhancing the material's thermal insulation performance [24, 25, 26]. For example, in the solar energy field, solar panels coated with polymer coatings can reduce heat loss and improve energy utilization efficiency [27, 28].

Polymer coatings are generally designed with special formulations, and their corrosion-resistant effects are manifested in corrosion resistance, wear resistance, and other aspects, with varying effectiveness depending on the material and process. Verma et al. [29] introduces the application of polymers as coating materials and reviews the application of polymer coatings in the biomedical and metal fields, including corrosion resistance, electrical conductivity, and other aspects, analyzing the two main components of corrosion-resistant coatings: solvents and adhesives. Xu et al. [30] points out that industrial equipment commonly faces corrosion prevention and heat dissipation issues. Based on this, it describes a novel high-thermal-conductivity and corrosion-resistant coating for heat exchanger protection, elucidating the mechanisms behind its enhanced thermal conductivity and corrosion resistance, thereby providing a reference for developing new functional coatings. Sharma and Sharma [31] reviews research on corrosion-resistant coatings based on urea-formaldehyde polymers (UFP), systematically introduces UFP and its properties, and discusses methods for preparing UFP composite coatings. Sun et al. [32] highlights the challenges in improving coating protective performance and designs a polyfluorophenylene/sodium dodecylbenzenesulfonate-cerium oxide montmorillonite (FA@SD-CeO_2–MMT) filler based on EP coatings. Experimental results reveal that FA@SD-CeO_2–MMT effectively enhances the corrosion resistance of EP coatings. Zhang et al. [33] points out the challenges in designing corrosion-resistant coatings suitable for harsh environments and, based on this, prepared a novel micro-network nano-filler CNTs/LDH-MoO_4 (CLM). Experimental verification demonstrated that CLM exhibits excellent corrosion-resistant performance in harsh environments. Chhipa, Sharma and Bagha [34] describes the effectiveness of polymer coatings in preventing corrosion and explores various methods for preventing metal corrosion, particularly the application of nanomaterials, conductive polymers, and nanocomposites in corrosion resistance.

The durability of polymer coatings is a critical factor determining the service life of metal products, influenced by factors such as specific types, usage scenarios, and maintenance conditions. Cirisano and Ferrari [35] aims to produce superhydrophobic surfaces using a simple and scalable method for producing polystyrene/polytetrafluoroethylene coatings, and verifies the durability of these films under harsh conditions such as high temperature and humidity, with potential for widespread application. Wu, Jayawickrama and Fujigaya [36] emphasizes that electrocatalysts made of high-crystallinity carbon materials are an effective method to enhance the durability of polymer electrolyte membrane fuel cells (PEMFCs), and experiments reveal that this method can effectively improve the durability and activity of PEMFCs. Zhang et al. [37] employs a simple method to enhance the durability and fuel cell performance of platinum electrocatalysts loaded on oxidized multi-walled carbon nanotubes, verifying that the polymer coating improves the durability of the electrocatalyst. Tuncer et al. [38] demonstrated that applying a polyester coating to coarse pumice aggregate and partially replacing uncoated aggregate with coated aggregate in lightweight concrete mixtures

improved the specific gravity of the aggregate but reduced its compressive strength. Peng et al. [39] developed a novel carbon capture (CC) coating made from calcium disilicate activated by carbon dioxide, which effectively enhances the durability of concrete structures and absorbs carbon dioxide, revealing the promising application prospects of CC coatings.

In terms of test systems, this paper sequentially selects four corrosion-resistant coating systems, their compositions, and the coating standards for test panel preparation. Regarding the analytical methods for corrosion-resistant coating performance, experiments and evaluation methods for coating porosity, corrosion resistance, and durability are designed based on the characteristics of high-temperature and high-humidity environments. Subsequently, using concrete as the test sample, the performance changes of the four corrosion-resistant coatings under high-humidity conditions are investigated, and the overall corrosion resistance of the four coatings is compared and analyzed. Subsequently, using the formulations of the selected four coating systems as a reference, a polymer-based sealing coating was prepared. The corrosion resistance of this coating was tested using salt spray and aqua regia materials. Finally, accelerated aging tests were conducted on the prepared polymer coating to verify its corrosion resistance in high-temperature and high-humidity environments. The durability of the coating material was evaluated by analyzing changes in its FTIR spectra.

2 | Test equipment

2.1 | Selection of corrosion protection systems

To gain a more comprehensive understanding of the performance and test results of various coating systems when subjected to high-temperature and high-humidity environments, this study systematically compares four well-established anti-corrosion coating systems, each sourced from different reputable manufacturers. For clarity and ease of discussion, these systems are designated as MN-1, MN-2, MN-3, and MN-4 throughout the analysis. The specific composition and formulation details for each coating system are provided as follows:

1) MN-1: Epoxy zinc-rich primer, epoxy micaceous iron oxide intermediate coat, acrylic aliphatic polyurethane topcoat.
2) MN-2: Epoxy zinc-rich primer, epoxy micaceous iron oxide intermediate coat, fluorocarbon topcoat.
3) MN-3: Epoxy zinc-rich primer, epoxy micaceous iron oxide intermediate coat, seawater-resistant series topcoat.
4) MN-4: Water-based epoxy anti-corrosion primer, water-based epoxy intermediate coat, water-based two-component polyurethane topcoat.

2.2 | Preparation of paint film

The specific coating requirements corresponding to each supporting system are comprehensively summarized in Table 1. In order to ensure experimental consistency and accuracy, all test panels should be prepared strictly in accordance with the technical specifications and parameters outlined in Table 1. When applying each layer of coating, it is important to maintain an interval of 36 hours between consecutive spray applications, allowing for proper setting and initial curing of the underlying layer. After the full curing period has elapsed for the final coat, the resulting thickness of the paint film should be carefully measured and verified to confirm that it falls within the target design range, thus ensuring the intended performance characteristics and durability of

the coating system are achieved.

TABLE 1 Coating requirements for each supporting system

Mating	Coating	Number of spray coats	Minimum dry film thickness(μm)	Total dry film thickness(μm)
MN-1	Primer coat	1	75	≧300
	Intermediate coat	1∼2	150	
	Finish coat	2	95	
MN-2	Primer coat	2	95	≧280
	Intermediate coat	2	130	
	Finish coat	2	75	
MN-3	Primer coat	1	65	≧250
	Intermediate coat	1	120	
	Finish coat	2	85	
MN-4	Primer coat	1	75	≧230
	Intermediate coat	2	140	
	Finish coat	1	65	
MN-5	The bottom and surface are integrated	2	90	≧150

3 | Analysis and research on coating performance

3.1 | Pore volume analysis method

There are various methods for measuring the porosity of coatings, such as direct weighing, optical microscopy, filter paper adhesion, impregnation, and spark testing. This study employs two methods: filter paper adhesion and spark testing.

The chemical reagents used in the filter paper method are potassium ferricyanide and sodium chloride solution. Among these, sodium chloride serves as the corrosive solution, used to corrode the sample, penetrating through the pores into the coating layer, reacting only with the base metal without corroding the surface. Potassium ferricyanide causes iron ions to turn blue and is used as an indicator.

In the experiment, a filter paper of size $3cm \times 3cm$ was placed at the center of the coating, and the prepared solution was dripped onto the filter paper until it was fully saturated. To ensure the filter paper adhered tightly to the coating and eliminate air bubbles, a tin plate was placed on top of the filter paper, followed by a 250g weight. After ten minutes, remove the filter paper, rinse it thoroughly with running water, and dry it with a hair dryer.

The determination of coating porosity is a critical parameter in assessing the protective performance of coatings applied to metallic substrates. In this study, the porosity of the coating was evaluated using a filter paper method, in which a test solution placed on filter paper is allowed to permeate through the pores of the coating, subsequently reacting with the underlying metal to produce visible blue spots. The number and distribution of these spots provide a quantitative measure of coating porosity. The porosity, P, is calculated as follows:

$$P = \frac{n}{S}, \tag{1}$$

where S denotes the area of the filter paper (cm^2), and n represents the total number of pore spots observed.

Given that the blue spots on the filter paper may vary in size, adjustments are implemented during the counting process: spots with diameters less than 1.15 mm are recorded as one pore, while those exceeding 1.15 mm in diameter are counted as two or three pores, depending on their specific size. The final porosity value for the coating is reported as the arithmetic mean from multiple independent measurements to ensure reliability and reproducibility.

In addition to the filter paper method, the spark testing technique was employed to further assess coating integrity. The DJ-VI type DC spark tester was utilized for this purpose. During testing, the probe of the instrument was systematically swept across the surface of the coating under a direct current high voltage. The presence of coating defects such as pinholes, bubbles, or cracks results in electrical breakdown and spark discharge, which is detected both visually and through an audible alarm. The measurement voltage (V) applied during spark testing is determined by the thickness (T_c) of the coating, with separate equations used for different thickness ranges:

For coatings with a thickness less than 1 mm:

$$V = 3294\sqrt{T_c} \tag{2}$$

For coatings with a thickness greater than or equal to 1 mm:

$$V = 7843\sqrt{T_c} \tag{3}$$

where V is the peak leakage voltage (V), and T_c is the thickness of the coating layer (mm).

3.2 | Corrosion resistance test method

Taking sulfuric corrosion experiments in oil pipelines as an example, the corrosion resistance testing method designed in this paper is as follows: the prepared samples are immersed in a prepared solution (containing sodium sulfide and sodium chloride, both with a mass fraction of 3.2%), and the temperature is set to a constant temperature of 45 and 65 for two groups. The uncoated parts of the samples are covered, and the immersion lasts for 12 days. The corrosion rate is determined using the weight loss method, and the corrosion grade can also be evaluated based on the corrosion morphology.

The **corrosion rate** is typically defined as the rate at which uniform or nearly uniform corrosion occurs across the entire exposed surface of a material. Among the various techniques available for quantifying corrosion, the weight loss test (often referred to as the weight loss method) is the most widely adopted. In this method, the corrosion rate is determined by measuring the reduction in sample mass per unit surface area over a specified time period. The corrosion rate, R_{Loss}, can be calculated as follows:

$$R_{\text{Loss}} = \frac{W_0 - W_1}{ST}, \tag{4}$$

where R_{Loss} represents the corrosion rate obtained via the weight loss method, in units of $g/(m^2 \cdot h)$; W_0 is the initial mass of the specimen before exposure to the corrosive environment, in grams; W_1 is the final mass after the completion of the test and removal of corrosion products, in grams; S denotes the exposed surface area of the sample, in m^2; and T corresponds to the total exposure duration, in hours.

To facilitate a more practical assessment of long-term corrosion, the weight loss rate can be converted to an annual corrosion rate using the following equation:

$$L = R_{\text{Loss}} \times \frac{8760}{\rho}, \tag{5}$$

where L is the average annual corrosion thickness of the coating (in m/a), R_{Loss} is the corrosion rate as determined above, but expressed in $kg/(m^2 \cdot h)$, 8760 is the number of hours in a year, and ρ is the measured density of the coating material (in kg/m^3).

It is important to note that the density, ρ, used in Eq. (5) should not be assumed as the theoretical density of the coating material. Instead, it should be experimentally determined. This is typically accomplished by weighing the coating sample with an electronic balance to obtain its mass, while its volume is measured using the displacement method, thereby enabling accurate calculation of the coating density.

3.3 | Methods for evaluating the durability of anti-corrosion coatings

3.3.1 | Salt spray test

Salt spray testing is a method used to evaluate the corrosion resistance of coatings by simulating the corrosive effects of salt spray in marine or harsh environments. During the test, metal plates coated with the test coating are placed in a sealed test chamber, where a high-concentration saltwater solution is atomized to create a salt spray environment. The samples are exposed to this environment for a specified period of time, typically measured in hours or days. The evaluation results primarily include the appearance of the coating, measurement of the corrosion extent of the coating, and inspection of the coating's adhesion. The corrosion extent of the coating is typically expressed in grades or levels, such as the C1 to C5 grades in the ASTM B117 standard. Higher grades indicate that the coating has better corrosion resistance.

3.3.2 | Wet heat cycle test

Wet heat cycling testing is a standard test method used to evaluate the durability of coatings and materials under high temperature and high humidity conditions. The principle behind this test is to simulate the application of coatings under different climatic conditions by alternately exposing samples to high temperature and high humidity environments and room temperature and low humidity environments, thereby testing the stability of the coating under these conditions. After the test, the appearance of the coating is observed for oxidation, blistering, peeling, or other defects, and the degree of corrosion of the coating is measured.

3.3.3 | Ultraviolet exposure test

Ultraviolet radiation in sunlight can cause coating fading, surface deterioration, and degradation. Therefore, the principle of ultraviolet exposure testing is based on the effects of ultraviolet radiation on coatings and materials, evaluating their weather resistance and aging resistance under ultraviolet radiation conditions. After testing, the main measurements are the degree of coating fading and surface deterioration, observing whether there is cracking, peeling, oxidation, etc.

3.3.4 | Wear testing

Wear testing methods, using agricultural machinery as an example, require agricultural machinery to operate under harsh field conditions, where it must withstand friction and wear from soil, stones, branches, and other objects. Therefore, the wear resistance of the coating directly impacts its field performance and service life. The principle of wear testing involves simulating the performance of coatings under mechanical wear or friction conditions to measure their wear resistance and durability. This helps determine whether coatings can withstand factors such as friction, wear, and scratches in actual use, thereby aiding in the selection of appropriate coating types and the improvement of coating formulations. This ensures that agricultural machinery maintains high performance and a long service life during field operations.

4 | Preparation of polymer coatings and study of their anti-corrosion effects

This section uses concrete as the experimental sample. By analyzing the changes in the surface coating's resistance to chlorine, sulfate ions, and carbon dioxide ions under high-humidity conditions, the overall corrosion resistance of the four corrosion protection systems is determined. Based on the corrosion resistance performance of the four corrosion protection systems, a polymer-based sealing coating was prepared and its corrosion resistance properties were tested. Furthermore, the aging behavior of the sealing agent coating under high-temperature and humid-heat conditions was investigated across six different substrates (measured by changes in coating material weight). By analyzing the FTIR spectra of the sealing agent coating under high-temperature and humid-heat conditions, the internal changes in the coating material were examined to validate the durability of the prepared polymer-based sealing agent coating.

4.1 | Changes in the performance of surface coating adhesion ions in high-humidity environments

4.1.1 | Chloride ion resistance

The changes in chloride ion resistance of four types of anti-corrosion coatings on concrete in a chloride ion environment are shown in Figure 1.

As shown in Figure 1, the chloride ion content decreases rapidly with increasing concrete depth. In the case of (C4) MN-1 corrosion-resistant coating, the chloride ion content on the concrete surface is 5.0%. When the concrete depth is 2 mm, the chloride ion content is 4.79%, and when the concrete depth is 4 mm, the chloride ion content is 4.08%. In contrast, the chlorine ion corrosion resistance of concrete containing MN-2 to MN-4 coatings is significantly stronger overall. Among the three coatings, the MN-3 corrosion-resistant coating provides the strongest improvement in concrete chlorine ion corrosion resistance, followed by the MN-4 coating, with the MN-2 coating being the weakest. When the concrete depth is 10 mm, the chloride ion content in (C1) MN-4 corrosion-resistant coating concrete is 0.54%, in (C2) MN-3 corrosion-resistant coating concrete is 0.31%, and in (C3) MN-2 corrosion-resistant coating concrete is 0.78%.

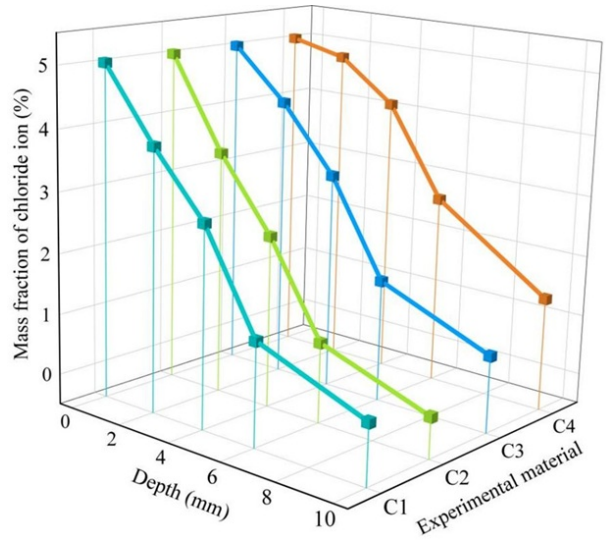

FIGURE 1 Changes in chloride ion resistance of four types of concrete

4.1.2 | Resistance to sulfate ions

Figure 2 shows the changes in the sulfate resistance of four types of anti-corrosion coatings on concrete in a sulfate ion environment.

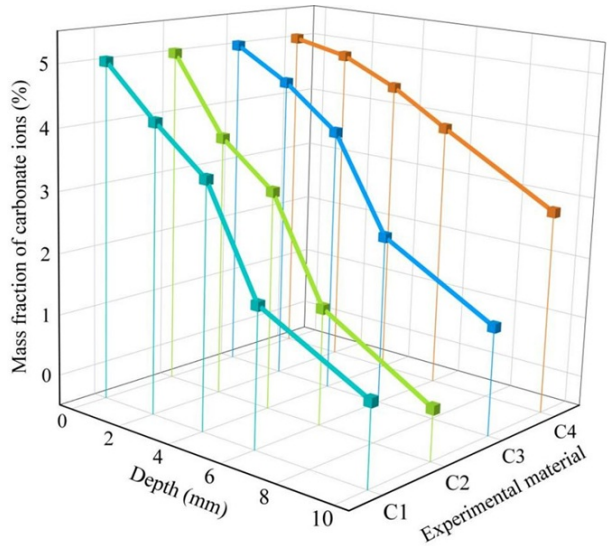

FIGURE 2 Changes in sulfate ion resistance of four types of concrete

Similar to the chloride ion environment, as the depth of the concrete increases, the sulfate ion content decreases rapidly. In the case of the (C4)MN-1 corrosion-resistant coating, the sulfate ion content at the

concrete surface reaches 5.00%. When the concrete depth is 2 mm, the sulfate ion content is 4.93%. When the concrete depth is 4 mm, the sulfate ion content is 4.62%. The remaining three corrosion-resistant coatings exhibit stronger resistance to sulfate ion corrosion. When the concrete depth is 10 mm, the sulfate ion content in concrete treated with (C1)MN-4 corrosion-resistant coating is 1.56%, the sulfate ion content of (C2)MN-3 corrosion-resistant coating concrete was 1.18%, and the sulfate ion content of (C3)MN-2 corrosion-resistant coating concrete was 1.94%. This is because the three corrosion-resistant coatings form a water-repellent molecular layer on the concrete surface and pore walls, which does not block the pores, thereby maintaining the original permeability of the concrete structure and enhancing its durability against sulfate ion corrosion.

Overall, the performance ranking of the four corrosion-resistant coatings in terms of concrete resistance to sulfate ion erosion is consistent with their resistance to chloride ions: MN-3 corrosion-resistant coating > MN-4 corrosion-resistant coating > MN-2 corrosion-resistant coating > MN-1 corrosion-resistant coating.

4.1.3 | Resistance to carbon dioxide

Figure 3 shows the changes in the carbonation resistance of four types of anti-corrosion coatings on concrete in a carbon dioxide environment.

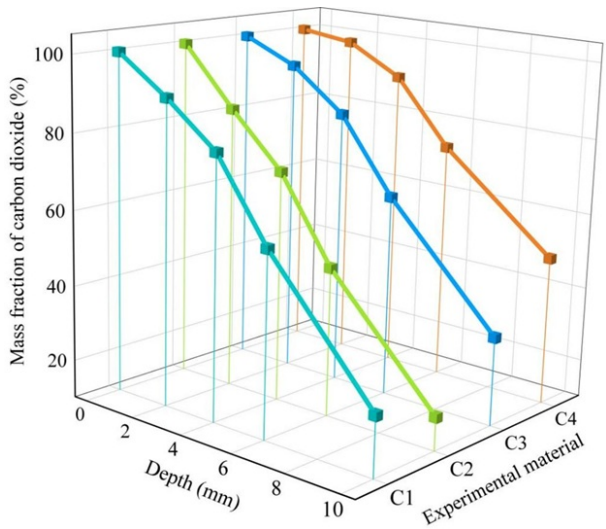

FIGURE 3 Changes in carbon dioxide resistance of four types of concrete

In a carbon dioxide environment, the concentration of carbon dioxide decreases rapidly as the depth of the concrete increases. In the case of (C4)MN-1 corrosion-resistant coating, when the depth of the concrete is 0 mm, the carbon dioxide concentration at the concrete surface is 100%. When the depth of the concrete is 2 mm, the carbon dioxide concentration is 97.58%. When the depth of the concrete increases to 4 mm, the carbon dioxide concentration decreases to 90.28%. When the concrete depth is 10 mm, the carbon dioxide ion content in (C1)MN-4 corrosion-resistant coating concrete is 25.69%, in (C2)MN-3 corrosion-resistant coating concrete it is 17.77%, and in (C3)MN-2 corrosion-resistant coating concrete it is 31.88%. These three corrosion-resistant coatings utilize the permeability of the concrete surface to penetrate into the concrete interior, where they

undergo in-situ reactions to form a solidified mass, filling the capillary pores and micro-cracks within the concrete, thereby enhancing the concrete's durability against carbon dioxide erosion.

Except for MN-1, the other three corrosion-resistant coatings form a dense corrosion-resistant layer on the concrete surface, preventing harmful substances from penetrating into the concrete interior, thereby enhancing the concrete's durability against chloride ion corrosion. MN-1, as a classic three-layer coating system, is susceptible to the influence of the testing environment, and once the topcoat's self-protective function fails, the coating system is prone to damage, resulting in its corrosion resistance being significantly inferior to that of the other three corrosion-resistant coating systems. Although MN-2 and MN-1 are both classic three-layer coating systems, MN-2 contains a fluorocarbon topcoat suitable for long-term use in high-temperature and high-humidity environments, featuring F-C chemical bonds and strong stability, resulting in overall performance superior to MN-2 corrosion-resistant coatings. Although the composition of the MN-3 corrosion-resistant coating system is identical to that of the MN-2 corrosion-resistant coating, the fluorocarbon topcoat formulation has been specially adjusted for high-temperature and high-humidity environments, making its corrosion resistance the best among the four coatings. The MN-4 corrosion-resistant coating uses water as the dispersing medium, offering higher safety and overall corrosion resistance superior to traditional MN-1 and MN-2 coatings, making it an environmentally friendly coating. In summary, the three corrosion-resistant coatings MN-2 to MN-4 all demonstrate a significant improvement in the concrete's resistance to chloride ion, sulfate ion, and carbon dioxide corrosion.

4.2 | Preparation and performance analysis of polymeric sealing coatings

Based on the analysis above, it can be concluded that the three types of anti-corrosion coatings MN-2 to MN-4 are effective in resisting corrosion in high-humidity environments. Therefore, this paper combines the raw materials of MN-2 to MN-4 anti-corrosion coatings to prepare a polymer sealer, which is then applied using an air spraying process to create an anti-corrosion sealing coating on the experimental substrate (copper sheet). This section briefly analyzes the chemical composition of the sealing coating and evaluates its corrosion resistance performance.

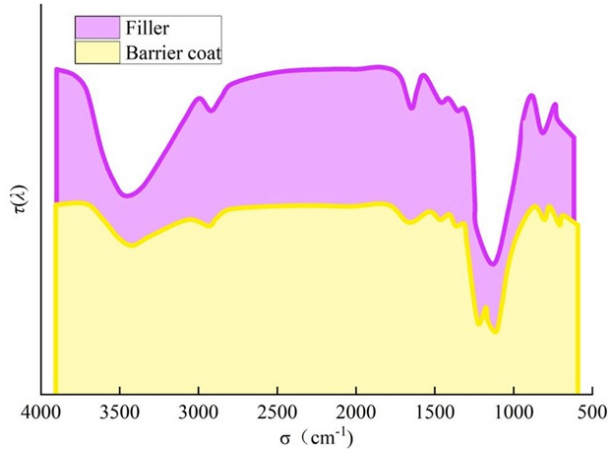

FIGURE 4 Infrared spectra of fillers and seal coating

4.2.1 | Chemical composition

The infrared spectra of the closed coating and filler are shown in Figure 4. The sealed coating exhibits absorption peaks of varying intensities at approximately 3469, 2907, 1666, 1213, 1157, and 1104 cm^{-1}. Among these, the absorption peaks at 3469, 2907, 1666, and 1104 cm^{-1} overlap with those of the filler, indicating that these peaks originate from the filler. The absorption peak at 1213 cm^{-1} in the sealed coating can be attributed to the C-F bonds in the modifier trifluoropropanol and the binder hexafluorobutyl acrylate. The presence of fluorine-containing groups effectively reduces the surface energy of the coating. The absorption peak at 1157 cm^{-1} is caused by the vibration of Si-O-Si bonds formed by the hydrolysis of TEOS. Its formation indicates that TEOS has been completely hydrolyzed, which further increases the roughness of the coating.

4.2.2 | Corrosion resistance

Copper plates coated with the sealing coating described in this paper and uncoated copper plates were subjected to salt spray corrosion simultaneously. The changes in mass of both types of plates are shown in Table 2. As the salt spray corrosion time increased, the mass of both types of copper plates decreased, with the uncoated copper plates experiencing a greater reduction in mass. After 4,000 hours of salt spray corrosion, the mass of the uncoated copper plates decreased by 43.8 g, representing a reduction of 52.33%. In contrast, the coated copper sheet only lost 4.8 g in mass, representing a reduction of just 5.72%. After 6,000 hours of salt spray corrosion, the coated copper sheet retained 77.7 g of its original mass, equivalent to 92.61% of its original mass, while the uncoated copper sheet retained only 24.85% of its original mass. It can be seen that under 5% sodium chloride salt spray corrosion conditions, copper sheets coated with a sealing coating exhibit excellent corrosion resistance compared to uncoated copper sheets, indicating that the sealing coating effectively slows down the corrosion of the copper sheet substrate by the salt spray.

TABLE 2 The quality changes of different copper sheets in salt spray tests

Salt spray corrosion time (h)	There are copper sheets with a closed coating(g)	Copper sheet without a closed coating(g)
0	83.9	83.7
1000	82.5	78.9
2000	79.9	69.4
3000	79.4	52.9
4000	79.1	39.9
5000	78.2	29.2
6000	77.7	20.8

The corrosion resistance of copper plates coated with a sealing agent and those without a sealing agent was tested using aqua regia. The changes in mass of both types of copper plates are shown in Table 3. As can be seen, the mass of both types of copper plates decreases as the corrosion time increases. By approximately 200 minutes into the aqua regia corrosion process, the copper sheet without a sealer was almost completely corroded by the aqua regia, with its total mass reduced to 0.6g, while the copper sheet with a sealer had only lost 10.1% of its mass. The mass loss of the copper sheet with a sealer was relatively slow within the first 200 minutes (19.11%). As time continued to elapse, the mass of the copper sheets coated with the sealing agent decreased

significantly compared to the initial mass, with only 9.9g remaining at 500 minutes, representing 11.06% of the original mass. The time it took for the copper sheets coated with the sealing agent to be completely corroded by aqua regia was delayed by at least 350 minutes compared to the uncoated copper sheets, demonstrating the sealing coating's exceptional corrosion resistance against aqua regia.

TABLE 3 The quality changes of different copper sheets immersed in aqua regia

Aqua regia corrosion time (min)	There are copper sheets with a closed coating(g)	Copper sheet without a closed coating(g)
0	83.9	83.5
1	83.8	83.5
5	83.8	83.4
10	83	81.7
20	82.2	76.8
60	81.4	60.2
100	79.6	32.5
150	75.5	2
200	68	0.6
300	43.9	
500	9.9	

4.3 | Analysis of the aging performance of polymeric sealing coatings

Combining the coating performance analysis research methods proposed in Chapter 3, six different substrates were selected as experimental samples (numbered 1-6 in order) to analyze the aging behavior of the polymer sealant developed in this paper under high temperature and high humidity conditions in this section, and to verify its anti-aging performance.

4.3.1 | Weight changes in accelerated aging sealant coatings under different conditions

1) *High-temperature accelerated aging test .* Test the weight loss of samples during the high-temperature aging test cycle. The test uses a balance with a precision of 0.001 g to measure the weight loss. Measurements are taken at intervals of 60°C for 72 hours (6 days). To ensure the accuracy of the test, the balance must be calibrated with weights before each group of samples is measured. Before weighing, the samples are placed in an indoor environment at 20°C with relative humidity of approximately 60% and left to rest for 12 hours to recover. The changes in sample weight under high-temperature aging are shown in Figure 5.

The weight changes of the six sample groups were all relatively small, around 0.025 g, and the weight loss trend remained consistent. During the first measurement cycle (60°C, 72 hours), the weight loss of the coated samples was significant (approximately 0.01 g), primarily due to mass loss caused by the evaporation of the liquid components of the composite coating. Around the aging time of (60°C, 300 hours), the sample weights no longer changed. Overall, under high-temperature aging test conditions, the weight state of the sealer coating material designed in this study remains relatively stable.

2) *Wet-heat accelerated aging.* Similar to the high-temperature aging test, before weighing, the samples were

placed in an indoor environment at 20°C with relative humidity of approximately 60% and left to rest for 12 hours to recover. Additionally, since the weight changes of the six groups of samples differed significantly from the total weight, the weight change trends were not clearly reflected. Therefore, the weight data was adjusted before the experiment. The weight changes of the samples under wet-heat aging are shown in Figure 6.

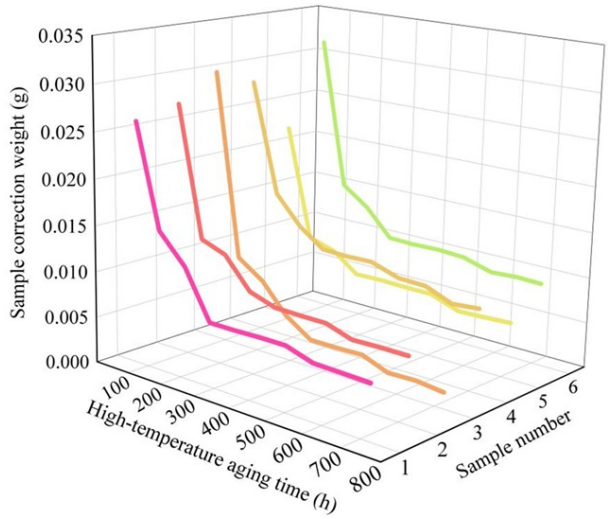

FIGURE 5 The weight change of samples due to accelerated aging at high temperatures

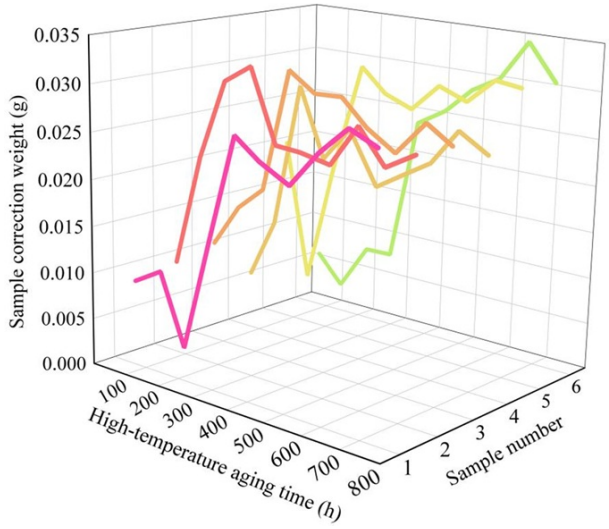

FIGURE 6 The weight change of samples with accelerated aging due to damp heat

Unlike the single-directional trend of mass loss observed in high-temperature aging, the weight of Sample 1 decreased during the first two test cycles of humidity-heat aging. At this point, the rate of moisture loss from the

coating exceeds the rate at which moisture molecules are absorbed in saturated steam concentration. However, by 300–400 hours (65°C), the weights of all six samples reached a stable state (0.020 g–0.035 g), indicating that the moisture absorption rate of the designed sealing agent coating samples had reached saturation. Under this condition, the weight gain of the samples ranged from 0.0171 g to 0.0283 g. Compared to the total weight of the samples (39.0 g to 50.0 g), the water absorption rate was relatively low, primarily due to the use of water-based materials in the protective coating, which allows water molecules to easily reach saturation within the material.

4.3.2 | FTIR analysis of sealing agent coating

To assess changes in the internal properties of the sealing agent material under artificially accelerated aging conditions, Fourier transform infrared spectroscopy (FTIR) was used to test samples exposed to high temperatures and humidity. The accelerated aging sealing agent coating samples were peeled off from the glass substrate surface, cut into 10×10 mm² test specimens, and tested using ATR-FTIR (Atomic Transmission Fourier Transform Infrared Spectroscopy). The high-temperature aging FTIR spectrum after baseline correction is shown in Figure 7, and the humid heat aging FTIR spectrum is shown in Figure 8.

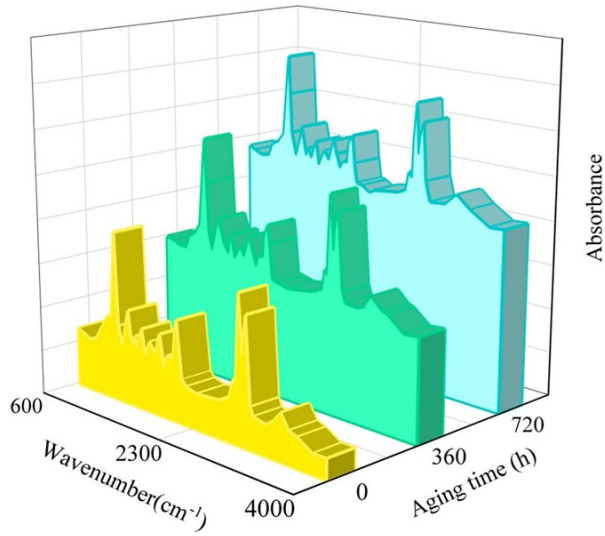

FIGURE 7 FTIR spectra of high-temperature aging

As shown in Figures 7 and 8, the broad peak at 3319 cm^{-1} is attributed to the stretching vibration of hydroxyl (-OH) groups in the sealer coating. The absorption peaks at 2947 cm^{-1} and 2857 cm^{-1} correspond to the stretching vibrations of methyl (-CH_3) and methylene (-CH_2) groups in the water-based coating. The absorption peak at 1720 cm^{-1} is attributed to the C=O stretching vibrations in the acrylic structure of the coating, while the peak at 1542 cm^{-1} corresponds to the C=C stretching vibrations in the acrylic resin of the coating. The absorption peaks in the range of 1037 cm^{-1} to 1284 cm^{-1} are caused by the stretching vibrations of the C-F bonds in the fluorocarbon components, and the absorption peak at 782 cm^{-1} is attributed to the γ phase of PVDF.

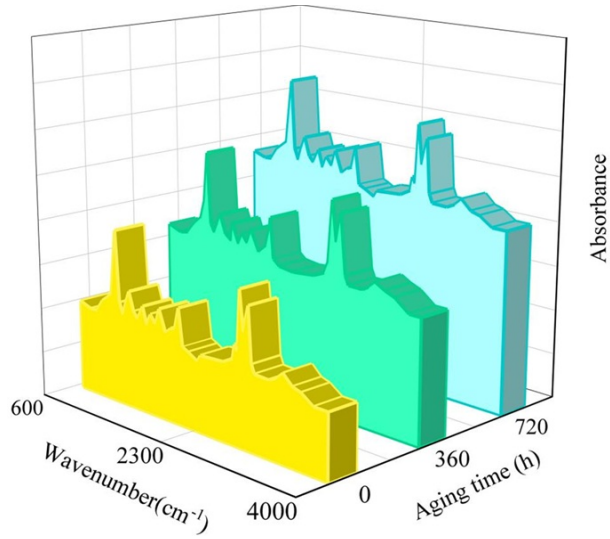

FIGURE 8 FTIR spectra of wet heat aging

Additionally, it can be observed that the molecular framework of the material has not undergone significant changes. The absorption peaks have not shifted toward the red or blue ends of the spectrum, no new absorption peaks have formed, and the intensity of the absorption peaks has not undergone significant changes. This indicates that no significant cross-linking chemical reactions have occurred within the material. After 60 days of cyclic aging, the chemical properties of the polymer coating prepared in this study have not undergone significant changes, and the coating has not experienced destructive failure.

5 | Conclusion

This study selected four established anti-corrosion coating products to evaluate the performance of various adhesive ions in surface coatings exposed to high humidity. The resulting anti-corrosion performance ranking was MN-3 > MN-4 > MN-2 > MN-1. Drawing on the raw material composition and their functional characteristics, a high-molecular anti-corrosion coating was developed, offering ease of application, high corrosion resistance, and strong durability under high-temperature, high-humidity conditions. The synthesized polymer sealant showed excellent protection in copper plate tests, retaining 92.61% of its mass after 6,000 hours of salt spray exposure and withstanding aqua regia corrosion for 300 minutes. Under high temperature and humidity, the weight change of the polymer coating was minimal, remaining within 0.025–0.035 g.

References

[1] Kausar, A. (2018). Polymer coating technology for high performance applications: Fundamentals and advances. *Journal of Macromolecular Science, Part A, 55*(5), 440-448.

[2] Cunningham, M. F., Campbell, J. D., Fu, Z., Bohling, J., Leroux, J. G., Mabee, W., & Robert, T. (2019). Future green chemistry and sustainability needs in polymeric coatings. *Green Chemistry, 21*(18), 4919-4926.

[3] Fu, C., Wang, Z., Gao, Y., Zhao, J., Liu, Y., Zhou, X., ... & Yang, P. (2023). Sustainable polymer coating for stainproof fabrics. *Nature Sustainability, 6*(8), 984-994.

[4] Wang, C., Wang, H., Li, M., Liu, Z., Lv, C., Zhu, Y., & Bao, N. (2018). Anti-corrosion and wear resistance properties of polymer composite coatings: Effect of oily functional fillers. *Journal of the Taiwan Institute of Chemical Engineers, 85*, 248-256.

[5] Shen, T., Liang, Z. H., Yang, H. C., & Li, W. (2021). Anti-corrosion coating within a polymer network: Enabling photothermal repairing underwater. *Chemical Engineering Journal, 412*, 128640.

[6] Rangel-Olivares, F. R., Arce-Estrada, E. M., & Cabrera-Sierra, R. (2021). Synthesis and characterization of polyaniline-based polymer nanocomposites as anti-corrosion coatings. *Coatings, 11*(6), 653.

[7] Kocacy, W. (2024). A Java-based framework for field inspection support systems in civil infrastructure. *TK Techforum Journal (ThyssenKrupp Techforum), 2024*(2), 7–14.

[8] Cui, G., Zhang, C., Wang, A., Zhou, X., Xing, X., Liu, J., ... & Lu, Q. (2021). Research progress on self-healing polymer/graphene anticorrosion coatings. *Progress in Organic Coatings, 155*, 106231.

[9] Sun, Y., Yuan, S., Fan, W., Lin, D., Zhang, K., Bai, Z., ... & Wang, H. (2023). A smart composite coating with photothermal response, anti-UV and anti-corrosion properties. *Chemical Engineering Journal, 452*, 138983.

[10] Weththimuni, M. L., Chobba, M. B., Sacchi, D., Messaoud, M., & Licchelli, M. (2022). Durable polymer coatings: A comparative study of PDMS-based nanocomposites as protective coatings for stone materials. *Chemistry, 4*(1), 60-76.

[11] Maan, A. M., Hofman, A. H., de Vos, W. M., & Kamperman, M. (2020). Recent developments and practical feasibility of polymer-based antifouling coatings. *Advanced Functional Materials, 30*(32), 2000936.

[12] Memon, H., De Focatiis, D. S., Choi, K. S., & Hou, X. (2021). Durability enhancement of low ice adhesion polymeric coatings. *Progress in Organic Coatings, 151*, 106033.

[13] Frigione, M. (2022). Assessment of the Ageing and Durability of Polymers. *Polymers, 14*(10), 1934.

[14] Anees, S. M., & Dasari, A. (2018). A review on the environmental durability of intumescent coatings for steels. *Journal of Materials Science, 53*(1), 124-145.

[15] Faccini, M., Bautista, L., Soldi, L., Escobar, A. M., Altavilla, M., Calvet, M., ... & Domínguez, E. (2021). Environmentally friendly anticorrosive polymeric coatings. *Applied Sciences, 11*(8), 3446.

[16] Ma, S., Ma, M., Huang, Z., Hu, Y., & Shao, Y. (2023). Research on the improvement of rainfall infiltration behavior of expansive soil slope by the protection of polymer waterproof coating. *Soils and Foundations, 63*(3), 101299.

[17] Al-Jabari, M. (2022). Waterproofing coatings and membranes. *Integral Waterproofing of Concrete Structures: Advanced Protection Technologies of Concrete by Pore Blocking and Lining*, 393.

[18] Tursunali o'g'li, Y. F. (2025). Technical principles and applications of polymer waterproof coatings. *Science, Education, Innovation: Modern Tasks and Prospects, 2*(2), 38-40.

[19] Gao, Y., Chang, X., & Shi, Y. (2024). Study on antibacterial durability of waterproof coatings with different base materials. *Construction Materials, 4*(3), 493-505.

[20] Ibraheim, S. M., & Hussein, S. I. (2020). Study on the contact angle, adhesion strength, and antibacterial activity of polymer/cement composites for waterproof coating. *Iraqi Journal of Science*, 1971-1977.

[21] Francke, B., & Wichowska, M. (2021). Influence of groundwater pH on water absorption and waterproofness of polymer modified bituminous thick coatings. *Materials, 14*(9), 2272.

[22] Xiong, A., & Li, J. (2024). Constructing stable transparent hydrophobic POSS@ epoxy-group coatings for waterproofing protection of decorative-painting surfaces. *Polymer Bulletin, 81*(2), 1403-1419.

[23] Ter-Zakaryan, K. A., Zhukov, A. D., Bobrova, E. Y., Bessonov, I. V., & Mednikova, E. A. (2021). Foam polymers in multifunctional insulating coatings. *Polymers, 13*(21), 3698.

[24] Ma, Z., Liu, X., Xu, X., Liu, L., Yu, B., Maluk, C., ... & Song, P. (2021). Bioinspired, highly adhesive, nanostructured polymeric coatings for superhydrophobic fire-extinguishing thermal insulation foam. *Acs Nano, 15*(7), 11667-11680.

[25] Ye, X., & Chen, D. (2018). Thermal insulation coatings in energy saving. *Energy-Efficient Approaches in Industrial Applications, 1.*

[26] Liu, L., Wang, C., & Liang, Q. (2022). Preparation of a heat insulation bonding layer for roads and its heat insulation effect. *Journal of Cleaner Production, 365*, 132828.

[27] Król, D., Motyl, P., Piotrowska-Woroniak, J., Patej, M., & Poskrobko, S. (2022). Heat reflective thin-film polymer insulation with polymer nanospheres—determination of thermal conductivity coefficient. *Energies, 15*(17), 6286.

[28] Hallad, S. A., Siddarath, B., Patil, A., Banapurmath, N. R., Kottursheттar, B. B., & Hunashyal, A. M. (2022). Development of thermal insulation coating for automotive application. *Materials Today: Proceedings, 59*, 1004-1008.

[29] Verma, A., Jain, N., Rastogi, S., Dogra, V., Sanjay, S. M., Siengchin, S., & Mansour, R. (2020). Mechanism, anti-corrosion protection and components of anti-corrosion polymer coatings. In *Polymer Coatings: Technologies and Applications* (pp. 53-66). CRC Press.

[30] Xu, F., Zhang, M., Cui, Y., Bao, D., Peng, J., Gao, Y., ... & Wang, H. (2022). A novel polymer composite coating with high thermal conductivity and unique anti-corrosion performance. *Chemical Engineering Journal, 439*, 135660.

[31] Sharma, N., & Sharma, S. (2021). Anticorrosive coating of polymer composites: A review. *Materials Today: Proceedings, 44*, 4498-4502.

[32] Sun, Y., Li, C., Fu, D., Hu, H., Bai, Z., Geng, H., ... & Wang, H. (2022). A novel high anti-corrosion performance polymer based composite coating with new functional fillers. *Progress in Organic Coatings, 162*, 106603.

[33] Zhang, M., Li, C., Wang, X., Peng, J., Yuan, S., Geng, H., ... & Wang, H. (2021). Ultrahigh anti-corrosion performance of polymer-based coating filled with a novel micro network nanofiller. *Corrosion Science, 190*, 109685.

[34] Chhipa, S. M., Sharma, S., & Bagha, A. K. (2024). Recent development in polymer coating to prevent corrosion in metals: A review. *Materials Today: Proceedings*.

[35] Cirisano, F., & Ferrari, M. (2021). Superhydrophobicity and durability in recyclable polymers coating. *Sustainability, 13*(15), 8244.

[36] Wu, D., Jayawickrama, S. M., & Fujigaya, T. (2022). Effect of polymer-coating on acetylene black for durability of polymer electrolyte membrane fuel cell. *Journal of Power Sources, 549*, 232079.

[37] Zhang, Q., Ling, Y., Cai, W., Yu, X., & Yang, Z. (2017). High performance and durability of polymer-coated Pt electrocatalyst supported on oxidized multi-walled in high-temperature polymer electrolyte fuel cells. *International Journal of Hydrogen Energy, 42*(26), 16714-16721.

[38] Tuncer, M., Bideci, A., Çomak, B., Durmuş, G., & Bideci, Ö. S. (2025). Experimental Investigation of Durability Properties of Polymer Coated Pumice Aggregate Lightweight Concretes. *Polymers, 17*(2), 253.

[39] Peng, L., Shen, P., Poon, C. S., Zhao, Y., & Wang, F. (2023). Development of carbon capture coating to improve the durability of concrete structures. *Cement and Concrete Research, 168*, 107154.